Tuning the Electronic Properties, Effective Mass and Carrier Mobility of MoS_2 Monolayer by Strain Engineering: First-Principle Calculations

Huynh V. Phuc, Nguyen N. Hieu, Bui D. Hoi, Nguyen V. Hieu, Tran V. Thu, Nguyen M. Hung, Victor V. Ilyasov, Nikolai A. Poklonski, et al.

Journal of Electronic Materials

ISSN 0361-5235
Volume 47
Number 1

Journal of Elec Materi (2018) 47:730-736
DOI 10.1007/s11664-017-5843-8

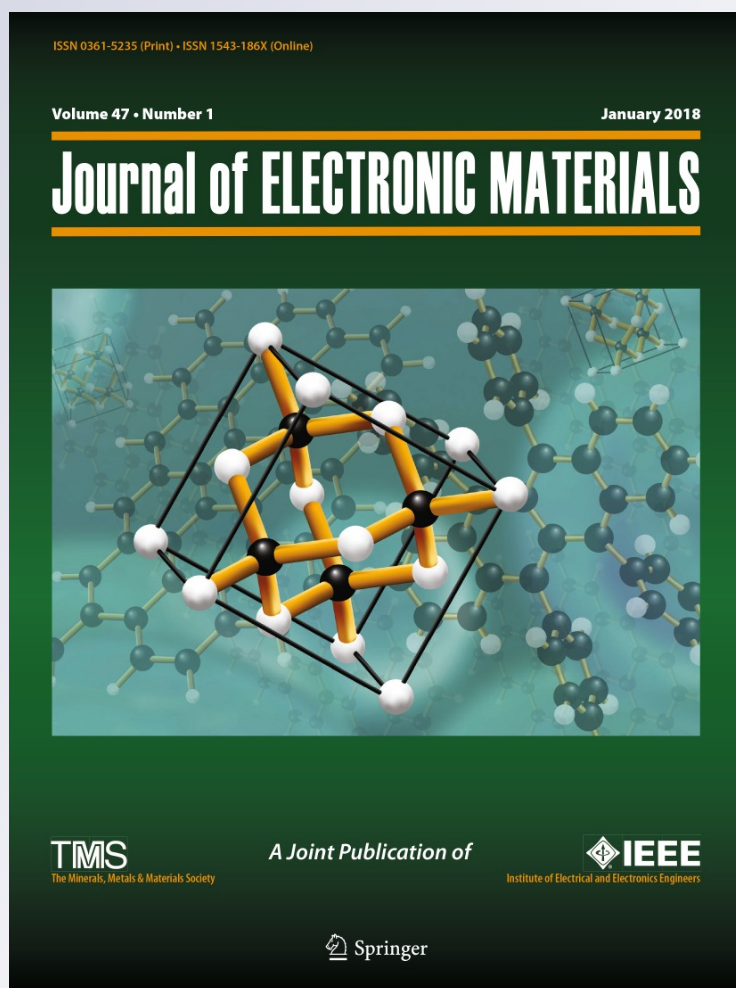

Springer

Your article is protected by copyright and all rights are held exclusively by The Minerals, Metals & Materials Society. This e-offprint is for personal use only and shall not be self-archived in electronic repositories. If you wish to self-archive your article, please use the accepted manuscript version for posting on your own website. You may further deposit the accepted manuscript version in any repository, provided it is only made publicly available 12 months after official publication or later and provided acknowledgement is given to the original source of publication and a link is inserted to the published article on Springer's website. The link must be accompanied by the following text: "The final publication is available at link.springer.com".

Springer

Author's personal copy

Journal of ELECTRONIC MATERIALS, Vol. 47, No. 1, 2018
DOI: 10.1007/s11664-017-5843-8
© 2017 The Minerals, Metals & Materials Society

CrossMark

Tuning the Electronic Properties, Effective Mass and Carrier Mobility of MoS_2 Monolayer by Strain Engineering: First-Principle Calculations

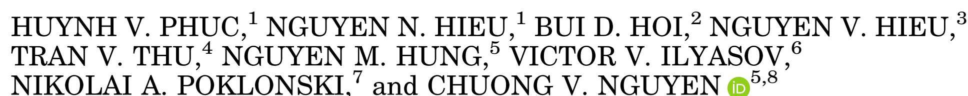
HUYNH V. PHUC,[1] NGUYEN N. HIEU,[1] BUI D. HOI,[2] NGUYEN V. HIEU,[3] TRAN V. THU,[4] NGUYEN M. HUNG,[5] VICTOR V. ILYASOV,[6] NIKOLAI A. POKLONSKI,[7] and CHUONG V. NGUYEN[5,8]

1.—Institute of Research and Development, Duy Tan University, Da Nang 550000, Vietnam. 2.—Department of Physics, University of Education, Hue University, Hue 530000, Vietnam. 3.—Department of Physics, University of Education, The University of Da Nang, Da Nang 550000, Vietnam. 4.—Department of Chemical Engineering, Le Quy Don Technical University, Ha Noi 100000, Vietnam. 5.—Department of Materials Science and Engineering, Le Quy Don Technical University, Ha Noi 100000, Vietnam. 6.—Department of Physics, Don State Technical University, Rostov on Don, Russia 344000. 7.—Physics Department, Belarusian State University, 220030 Minsk, Belarus. 8.—e-mail: chuongnguyen11@gmail.com

In this paper, we studied the electronic properties, effective masses, and carrier mobility of monolayer MoS_2 using density functional theory calculations. The carrier mobility was considered by means of *ab initio* calculations using the Boltzmann transport equation coupled with deformation potential theory. The effects of mechanical biaxial strain on the electronic properties, effective mass, and carrier mobility of monolayer MoS_2 were also investigated. It is demonstrated that the electronic properties, such as band structure and density of state, of monolayer MoS_2 are very sensitive to biaxial strain, leading to a direct–indirect transition in semiconductor monolayer MoS_2. Moreover, we found that the carrier mobility and effective mass can be enhanced significantly by biaxial strain and by lowering temperature. The electron mobility increases over 12 times with a biaxial strain of 10%, while the carrier mobility gradually decreases with increasing temperature. These results are very useful for the future nanotechnology, and they make monolayer MoS_2 a promising candidate for application in nanoelectronic and optoelectronic devices.

Key words: MoS_2 monolayer, band gap, strain engineering, mobility, DFT calculations

INTRODUCTION

Two-dimensional (2D) materials, especially graphene,[1,2] have attracted great interest for applications in nanoelectronic and optoelectronic devices owing to their unique properties.[3] However, graphene is a semimetal with zero band gap,[4] which limits its applications in graphene-based electronic devices, such as field effect transistors (FETs). Recently, molybdenum disulfide (MoS_2) has been recognized as a promising material for applications in nanoelectromechanical devices due to its extraordinary mechanical, electronic and transport properties.[5–9] MoS_2 monolayer can be fabricated by various experimental methods, such as chemical vapor deposition[10,11] or a microexfoliation technique which has been used to produce graphene.[12] In contrast to graphene, which is semimetallic with zero band gap, monolayer MoS_2 is a semiconductor with a natural band gap.[13] Thus, monolayer MoS_2 can be useful for such applications as field effect transistors with excellent current on/off ratios (10^8)[14] and highly sensitive photodetectors.[15]

(Received August 4, 2017; accepted September 27, 2017; published online October 16, 2017)

Author's personal copy

Many theoretical research groups have studied the properties of monolayer MoS_2 using first-principles calculations. They focused on the electronic,[16–18] elastic,[19] and optical properties[20–23] of MoS_2. The functionalization through adatom,[24,25] molecular adsorption,[26] and vacancy defect creation[27–29] in MoS_2 have been also investigated by different methods. In addition, the effect of strain on electronic states and optical properties of monolayer MoS_2 has been considered both theoretically and experimentally.[30–34] Lloyd and co-workers[33] experimentally studied the effect of ultra-large biaxial strain on the band gap of monolayerMoS_2 .The effect of local strain on the band structure of multilayer 2D transition-metal di-chalcogenide (TMD) materials has been investigated both theoretically and experimentally by Dhakal's group.[34] The stability and electronic and magnetic properties of MoS_2 nanoribbons have also been investigated.[35] Recently, we systematically investigated the electronics of monolayer MoS_2 using density functional theory (DFT) calculations.[36] Effects of the in-plane (*xy* plane) biaxial strain on electronic properties have also been considered.[36] In the present work, we estimate the fluctuation of the carrier effective mass in 2D monolayer MoS_2 under small strain. The role of strain in the change of the electronic and transport properties of monolayer MoS_2 is also investigated. Our results may be useful for applications of monolayer MoS_2 in electronic and optoelectronic devices.

THEORETICAL MODEL AND METHOD

The *ab initio* calculation was performed with the DFT method using generalized gradient approximation (GGA)[37] for the exchange-correlation energy, which is implemented in the Quantum Espresso package.[38] The GGA with Perdew-Burke-Ernzerhof (PBE) exchange-correlation potential was used with projected augmented wave. The electronic wavefunctions were described by a plane wave basis set with an energy cutoff of 410 eV. The Brillouin zone sampling with the Monkhorst-Pack method of $(9 \times 9 \times 1)$ Monkhorst-Pack k-grid mesh was chosen for the calculations. A vacuum layer of 20 Å in thickness was added on the top of the monolayer MoS_2 to avoid interaction between layers. The structure is fully relaxed with an energy convergence of 10^{-6} eV and a force convergence of 0.01 eV/Å.

A scheme of the monolayer MoS_2 with hexagonal symmetry under biaxial strain is shown in Fig. 1. The strained cell is designed by stretching the hexagonal ring in the *xy* plane. The strain engineering is applied in a biaxial expansion along the *xy*-direction. The component of biaxial strain is denoted by ε. In the present work, a wide range of strain (up to 10%) was employed.

At room temperature, the electron velocity υ was of the magnitude of 10^7 cm/s. The lattice constant of

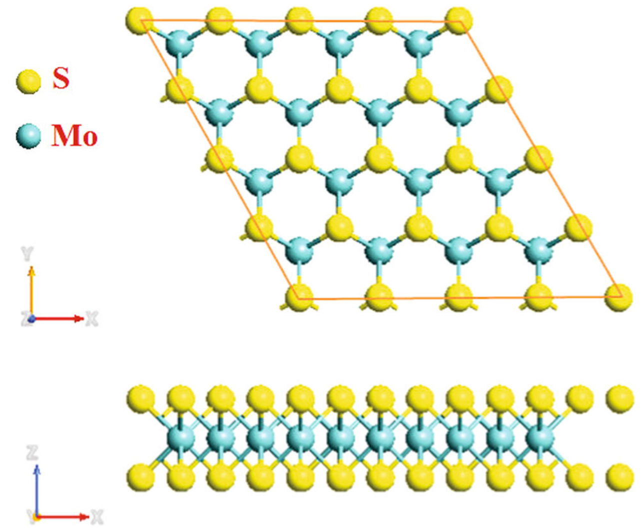

Fig. 1. Top (a) and side (b) views of the relaxed atomic structure of MoS_2 monolayer.

monolayer MoS_2 was much smaller than the wavelength of the electron ($\lambda \approx 7$ nm). Hence, we believe that the delocalized charge was scattered only by the acoustic phonons and we can use the deformation potential theory proposed by Bardeen and Shockley[39] to describe this scattering process. In the effective mass approximation and electron-acoustic phonon scattering mechanism in a 1D system, the mobility can be defined via the average value of the momentum relaxation time τ as follows[40]

$$\mu_{2D} = \frac{e\tau}{m^*} = \frac{2e\hbar^3 C}{3k_B T|m^*|^2 E_1^2}, \tag{1}$$

where E_1 is the deformation potential constant denoting the shift of the valence band maximum for holes and the conduction band minimum for electrons, e is the electron charge, $m^* = \hbar^2(\partial^2 E/\partial k^2)^{-1}$ is the effective mass of the charge, k_B is the Boltzmann constant, $T = 300$ K is the temperature in the present calculations, and C is the stretching modulus of the crystal for simulating the lattice distortion activated by strain. The stretching modulus for the 2D system is $C^{2D} = [\partial^2 E/\partial \delta^2]/S_0$, where E is total energy of the system, δ is the applied uniaxial strain, and S_0 is the area of the optimized structure. To consider the effect of the temperature on mobility, we calculate the carrier mobility of MoS_2 at several temperatures in the range from 100 K to 400 K.

RESULTS AND DISCUSSION

We first investigated the electronic properties of the monolayer MoS_2 using DFT calculations. We used the GGA to optimize the geometry of the monolayer MoS_2. The atomic structure and the model of the applied strain engineering of the

Author's personal copy

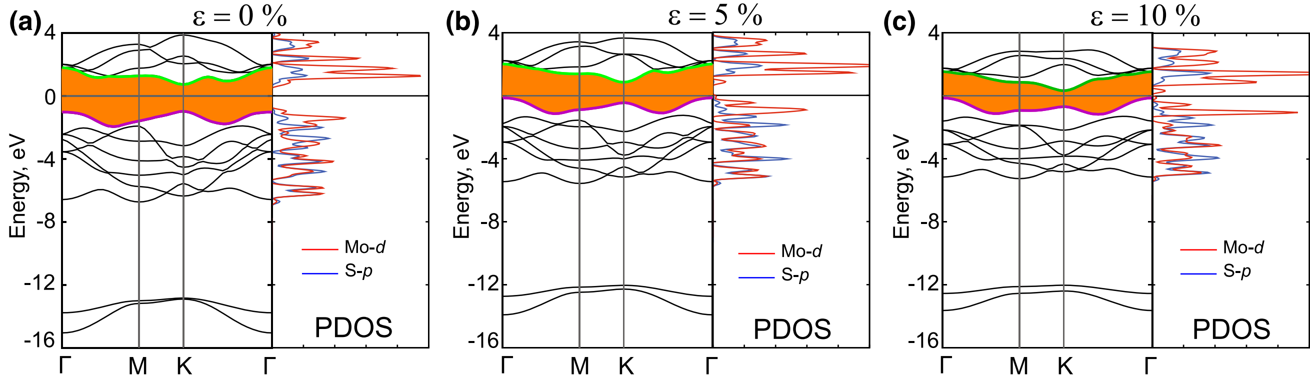

Fig. 2. Band structures and PDOS of monolayer MoS_2 with the applied strains of 0 % (a), 5 % (b) and 10 % (c). The Fermi level is set to 0 eV. In the band structure, the purple and green lines stand for the valence band maximum and the conduction band minimum of MoS_2 monolayer, respectively.

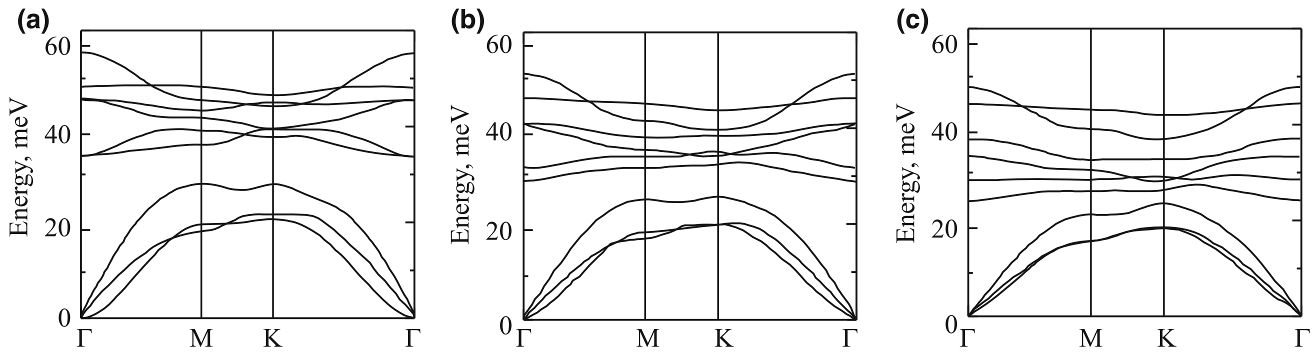

Fig. 3. Phonon dispersion curves of MoS_2 monolayer under biaxial strains of 0 % (a), 5 % (b), and 10 % (c).

monolayer MoS_2 are illustrated in Fig. 1. At the equilibrium state, the lattice constant is equal to 3.18 Å and the bond distance between S and Mo atoms is 2.42 Å. This result is in good agreement with the previous theoretical[41,42] and experimental[43] studies. Based on DFT calculations, we see that, in the equilibrium state, the monolayer MoS_2 is a direct semiconductor with band gap of 1.72 eV. This direct band gap is close to the result of the previous DFT calculations by Matte and co-workers.[44] It is well-known that the traditional DFT method underestimates the band gap of materials, however, this trend is not general and depends on the materials considered.[45,46] The band gap problem can be addressed more accurately by using a GW approximation or hybrid functionals.[27] Hence, we believe that our calculated DFT method is a suitable method for considering the transport properties of monolayerMoS_2 .

In Fig. 2a, we show the electronic energy band structure and partial density of states (PDOS) of Mo-*d* and S-*p* orbitals in monolayer MoS_2 at the equilibrium state. At the equilibrium state, the direct band gap of monolayer MoS_2 is at the K point. The lowest energy of the conduction band and the highest energy of the valence band in monolayer MoS_2 are located at the K point. At equilibrium, the main contributor to the bottom of the conduction band is the Mo-*d* orbitals, and the contributors to the roof of the valence band are the Mo-*d* and S-*p* orbitals. Mo-*d* and S-*p* orbitals are hybridized with each other at the top of the valence band. This character indicates that the Mo–S bond is strong. However, the mirror symmetrical bonding configuration in the trilayer S–Mo–S system results in a weak π bond-like interaction. This weak interaction is very sensitive to strain, leading to a change of band structure in the presence of strain, as shown in Fig. 2b and c.

Our calculations demonstrate that biaxial strain along the *xy*-direction has a significant effect on the band gap and PDOS of monolayer MoS_2 (see Fig. 2). The electronic properties of MoS_2 are particularly sensitive to the mechanical strain. Under biaxial strain, monolayer MoS_2 becomes an indirect gap semiconductor. The lowest energy of the conduction band is still located at the *K* point, while the highest energy of the valence band is now at the Γ point in the reciprocal lattice space. We can also easily see that a direct–indirect gap transition can be found when biaxial strain is applied, as shown in Fig. 2. A shift of energy levels leads to a change in the nature of the energy band gap of the monolayer MoS_2 from direct to indirect, even in the case of biaxial strain of

Author's personal copy

Table I. Deformation potential constant E_1 (eV), stretching modules C^{2D} (N/m), effective mass m^* (m_0), relaxation time τ (fs), and mobility μ (cm^2/Vs) of carriers in monolayer MoS_2

	E_1	C^{2D}	m^*	τ	μ
Electron	11.02	138.2	0.454	20.05	77.30
Hole	5.05	138.2	0.626	69.25	193.60

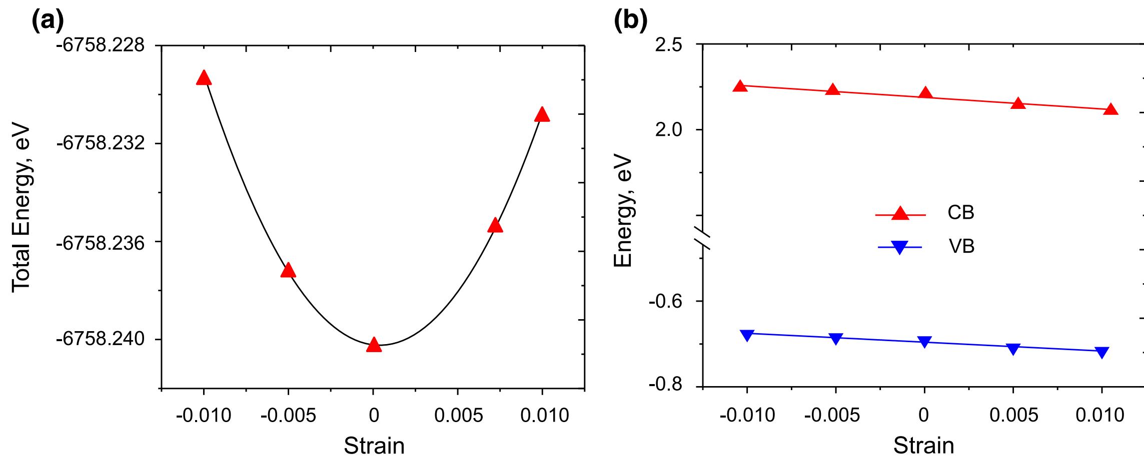

Fig. 4. Dependence of total energy (a) and shifts of the conduction band (CB) and the valence band (VB) (b) of MoS_2 under biaxial strain.

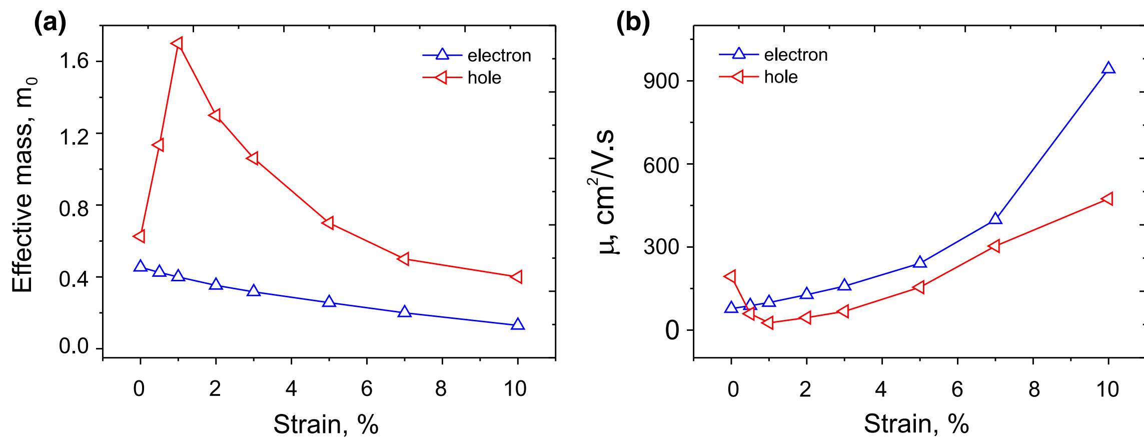

Fig. 5. The carrier effective mass (a) and the carrier mobility (b) as function of biaxial strain.

less than 1%. This means that, in the presence of biaxial strain, the monolayer MoS_2 is an indirect semiconductor. The band gap of monolayer MoS_2 decreases from 1.72 eV to 0.46 eV when the applied strain increases from 0% to 10%. Our calculations also show that with the increasing strain, the valence band maximum is upshifted and the conduction band minimum downshifted, resulting in a decrease of the band gap as shown in Fig. 2.

To consider the structural stability of MoS_2 monolayer under biaxial strain, we also calculate the phonon dispersion curves of monolayerMoS_2 at the equilibrium state (unstrained) and under biaxial strain, as shown in Fig. 3. The phonon dispersion curves of monolayerMoS_2 without strain count nine phonon modes, as shown in Fig. 3a, which is in complete agreement with the previous results.[47] Under biaxial strain, we can see that the phonon dispersion curves of monolayerMoS_2 are gradually downshifted, resulting in a decrease of the gap between the acoustic and optical branches. As shown in Fig. 3c, we can see that the structure of monolayerMoS_2 is still stable under biaxial strain of 10%.

Next, via the effective mass approximation and electron–acoustic phonon scattering mechanism, we

Author's personal copy

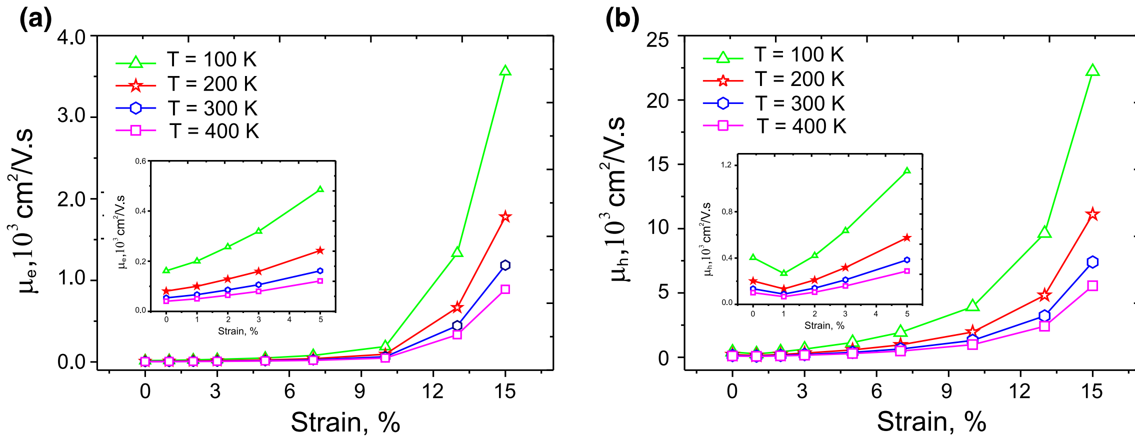

Fig. 6. Dependence of the electron (a) and hole (b) mobility at different temperatures on strain. The insets are the zoom in the strain range from 0% to 5%.

investigate the transport properties of monolayer MoS_2 with and without mechanical strain. To calculate the carrier mobility, we first calculate the effective mass m^*, the stretching modulus C^{2D}, and the deformation potential constant E_1. In Table I, we show these parameters at the equilibrium state of monolayer MoS_2. Figure 4a shows the dependence of the total energy on the small strain applied along the x direction. The stretching modulus C^{2D} is obtained by fitting the energy-strain curves. Figure 4b shows the shift of the band edges as a function of strain along the x direction. As shown in Table I, the stretching modulus of monolayer MoS_2 at the equilibrium state is 138.2 N/m. These data are in excellent agreement with the previous theoretical calculations by Y. Cai and coworkers.[48] Based on the band structure, we can fit two curves for the top of the valence band and the bottom of the conduction band at the Fermi energy level, whence we get the effective masses m_e and m_h for electron and hole, respectively. Our calculations show that, at equilibrium, the effective masses for electron m_e and hole m_h are $0.454m_0$ and $0.626m_0$, respectively. These values are in good agreement with previous theoretical studies.[48,49]

The change of the effective mass under strain of monolayer MoS_2 is illustrated in Fig. 5a. The effective mass of monolayer MoS_2 can be controlled by applying biaxial strain. As shown in Fig. 5a, the electron carrier effective mass depends linearly on the biaxial strain. The effective mass of the electron decreases when the biaxial strain increases. The effective mass of the electron drops from $0.454m_0$ to $0.257m_0$, and to $0.13m_0$ by applying biaxial strains of 0% (unstrained state), 5% and 10%, respectively. Meanwhile, the effective mass of holes experiences a fluctuation as the strain increases. The fluctuation is caused by the valence band maximum (VBM) jumping from the K point to the Γ point during the strain induced deformation of the band structure or direct-to-indirect band gap at a strain of 1%.

The effective mass of holes is $0.626m_0$ at the equilibrium state but abruptly jumps to $1.721m_0$ with an applied strain of 1%, and then strongly decreases when the applied strain $\varepsilon > 1\%$. When the strain further increases, the effective mass of holes begins decreasing to $0.4m_0$ at a strain of 10%. Besides, the effective mass of holes is slightly larger than that of electrons in all cases of biaxial strain.

We next investigate the electron and hole mobilities of monolayer MoS_2 under strain at a room temperature of 300 K. At this temperature, the hole and electron mobilities are respectively 193.60 cm^2/Vs and 77.30 cm^2/Vs . These values are in good agreement with previous theoretical studies.[48] The dependence of the mobility on strain is illustrated in Fig. 5b. We found that the electron mobility monotonically increases with increasing strain, whereas the hole mobility reaches a minimum at a biaxial strain of 1%, then also increases with increasing strain. The electron mobility increases from 77.30 cm^2/Vs to 241.21 cm^2/Vs by three times and to 942.73 cm^2/Vs by 12 times, when strain increases from 0% to 5% and 10%, respectively. The hole mobility exhibits a large reduction from 193.60 cm^2/Vs to 26.25 cm^2/Vs when the strain increases from 0% to 1%. This reduction is caused by the direct-to-indirect band gap transition with the valence band shifting from the K point to the Γ point at the strain of 1%. When the strain further increases, the hole mobility begins to increase and reaches 474.17 cm^2/Vs when increasing strain to 10%. Figure 5b also shows that the hole mobility is slightly larger than the electron mobility in the unstrained state, but becomes smaller with biaxial strain.

Additionally, the carrier mobilities of electrons and holes of monolayer MoS_2 at various temperatures (100 K, 200 K, 300 K, and 400 K) are also considered. Figure 6a and b illustrate the temper-

Author's personal copy

ature dependent carrier mobilities under strain. The electron mobility of monolayer MoS_2 under a strain of 10% increases from 707 cm^2/Vs at $T = 400$ K to 2800 cm^2/Vs at $T = 100$ K, whereas, at the equilibrium state, the hole mobility decreases from 580.80 cm^2/Vs to 145.20 cm^2/Vs when the temperature increases from 100 K to 400 K. Our study indicates that the carrier mobility is inversely proportional to the temperature. As mentioned above, the relaxation time for acoustic phonon scattering is independent of the carrier energy, and they depend on the temperature. Thus, according to Eq. 1, it indicates that the mobility acquires a $\mu \sim T^{-1}$ dependence characteristic for 2D systems and layered materials dominated by acoustic phonon scattering. Our study also shows a very interesting observation with detailed information on the effects of strain on the carrier effective mass and mobility in monolayer MoS_2, which is very helpful for the future of MoS_2 for applications in nanoscale electronics and photonics devices.

CONCLUSION

In summary, by using density functional theory, we investigated the effects of biaxial strain on the electronic properties, effective masses and carrier mobilities of 2D monolayer MoS_2. It was demonstrated that the electronic and transport properties of monolayer MoS_2 are very sensitive to biaxial strain. The results showed that the band gap of monolayer MoS_2 is reduced monotonically when increasing biaxial strain. Furthermore, we found the direct-to-indirect band gap transition in monolayer MoS_2 by applying biaxial strain of $E_b \geq 1\%$. At the unstrained state the effective masses and carrier mobility for electron (hole) of monolayer MoS_2 are $0.454m_0$ ($0.626m_0$) and 77.30 cm^2/Vs (193.60 cm^2/Vs), respectively. Moreover, we have found that the carrier mobility can be enhanced significantly by biaxial strain and by lowering temperature. These results supply a fascinating observation with detailed information on the effect of biaxial strain on carrier effective mass and mobility in monolayer MoS_2, which is very helpful for future applications of monolayer MoS_2 in nanoelectronic and optoelectronic devices.

ACKNOWLEDGEMENTS

This research is funded by Vietnam National Foundation for Science and Technology Development (NAFOSTED) under Grant Number 103.01-2016.07 and the Belarusian Scientific Program "Convergence".

CONFLICT OF INTEREST

The authors declare that they have no conflict of interest.

REFERENCES

1. A.K. Geim and K.S. Novoselov, *Nat. Mater.* 6(3), 183 (2007).
2. K. Novoselov, A. Geim, S. Morozov, D. Jiang, M. Katsnelson, I. Grigorieva, S. Dubonos, and A. Firsov, *Nature* 438(7065), 197 (2005).
3. Q. Tang, Z. Zhou, and Z. Chen, *WIREs Comput. Mol.* Sci 5(5), 360 (2015).
4. A.C. Neto, F. Guinea, N.M. Peres, K.S. Novoselov, and A.K. Geim, *Rev. Mod. Phys.* 81(1), 109 (2009).
5. M. Chhowalla, H.S. Shin, G. Eda, L.J. Li, K.P. Loh, and H. Zhang, *Nat. Chem.* 5(4), 263 (2013).
6. A.M. van der Zande, P.Y. Huang, D.A. Chenet, T.C. Berkelbach, Y. You, G.H. Lee, T.F. Heinz, D.R. Reichman, D.A. Muller, and J.C. Hone, *Nat. Mater.* 12(6), 554 (2013).
7. Y. Li, D. Wu, Z. Zhou, C.R. Cabrera, and Z. Chen, *J. Phys. Chem. Lett.* 3(16), 2221 (2012).
8. Y. Jing, E.O. Ortiz-Quiles, C.R. Cabrera, Z. Chen, and Z. Zhou, *Electrochim. Acta* 147, 392 (2014).
9. C.V. Nguyen, N.N. Hieu, N.A. Poklonski, V.V. Ilyasov, L. Dinh, T.C. Phong, L.V. Tung, and H.V. Phuc, *Phys. Rev. B* (accepted for publication) (2017).
10. K.K. Liu, W. Zhang, Y.H. Lee, Y.C. Lin, M.T. Chang, C.Y. Su, C.S. Chang, H. Li, Y. Shi, H. Zhang, et al., *Nano Lett.* 12(3), 1538 (2012).
11. Y.H. Lee, X.Q. Zhang, W. Zhang, M.T. Chang, C.T. Lin, K.D. Chang, Y.C. Yu, J.T.W. Wang, C.S. Chang, L.J. Li, et al., *Adv. Mater.* 24(17), 2320 (2012).
12. R.J. Smith, P.J. King, M. Lotya, C. Wirtz, U. Khan, S. De, A. O'Neill, G.S. Duesberg, J.C. Grunlan, G. Moriarty, et al., *Adv. Mater.* 23(34), 3944 (2011).
13. K.F. Mak, C. Lee, J. Hone, J. Shan, and T.F. Heinz, *Phys. Rev. Lett.* 105(13), 136805 (2010).
14. B. Radisavljevic, A. Radenovic, J. Brivio, I.V. Giacometti, and A. Kis, *Nat. Nanotechnol.* 6(3), 147 (2011).
15. Z. Yin, H. Li, H. Li, L. Jiang, Y. Shi, Y. Sun, G. Lu, Q. Zhang, X. Chen, and H. Zhang, *ACS Nano* 6(1), 74 (2011).
16. S. Lebegue and O. Eriksson, *Phys. Rev. B* 79(11), 115409 (2009).
17. E. Scalise, M. Houssa, G. Pourtois, V. Afanasev, and A. Stesmans, *Nano Res.* 5(1), 43 (2012).
18. L. Dong, R.R. Namburu, T.P. ORegan, M. Dubey, and A.M. Dongare, *J. Mater. Sci.* 49(19), 6762 (2014).
19. L. Wei, C. Jun-fang, H. Qinyu, and W. Teng, *Physica B* 405(10), 2498 (2010).
20. W.B. Xu, B.J. Huang, P. Li, F. Li, C.w. Zhang, and P.J. Wang, *Nanoscale Res. Lett.* 9(1), 1 (2014).
21. A. Kumar and P. Ahluwalia, *Mater. Chem. Phys.* 135(2), 755 (2012).
22. H. Shi, H. Pan, Y.W. Zhang, and B.I. Yakobson, *Phys. Rev. B* 87(15), 155304 (2013).
23. K.P. Dhakal, D.L. Duong, J. Lee, H. Nam, M. Kim, M. Kan, Y.H. Lee, and J. Kim, *Nanoscale* 6(21), 13028 (2014).
24. L.P. Feng, J. Su, S. Chen, and Z.T. Liu, *Mater. Chem. Phys.* 148(1), 5 (2014).
25. W. Shi, Z. Wang, Z. Li, and Y.Q. Fu, *Mater. Chem. Phys.* 183, 392 (2016).
26. Y. Jing, X. Tan, Z. Zhou, and P. Shen, *J. Mater. Chem. A* 2(40), 16892 (2014).
27. C. Ataca and S. Ciraci, *J. Phys. Chem. C* 115(27), 13303 (2011).
28. Y. Wang, S. Li, and J. Yi, *Sci. Rep.* 6 (2016).
29. Z. Wang, Q. Su, G. Yin, J. Shi, H. Deng, J. Guan, M. Wu, Y. Zhou, H. Lou, and Y.Q. Fu, *Mater. Chem. Phys.* 147(3), 1068 (2014).
30. M. Nayeri, M. Fathipour, and A.Y. Goharrizi, *J. Phys. D Appl. Phys.* 49(45), 455103 (2016).
31. A. Sengupta, R.K. Ghosh, and S. Mahapatra, *IEEE Trans. Electron Dev.* 60(9), 2782 (2013).
32. L. Yang, X. Cui, J. Zhang, K. Wang, M. Shen, S. Zeng, S.A. Dayeh, L. Feng, and B. Xiang, *Sci. Rep.* 4 (2014).

Author's personal copy

33. D. Lloyd, X. Liu, J.W. Christopher, L. Cantley, A. Wadehra, B.L. Kim, B.B. Goldberg, A.K. Swan, and J.S. Bunch, *Nano Lett.* 16(9), 5836 (2016).
34. K.P. Dhakal, S. Roy, H. Jang, X. Chen, W.S. Yun, H. Kim, J.D. Lee, J. Kim, and J.H. Ahn, *Chem. Mater.* 6, 13028 (2014).
35. Y. Li, Z. Zhou, S. Zhang, and Z. Chen, *J. Am. Chem. Soc.* 130(49), 16739 (2008).
36. C.V. Nguyen, V.V. Ilyasov, H.V. Nguyen, and H.N. Nguyen, *Mol. Simul.* 43(2), 86 (2017).
37. J.P. Perdew, K. Burke, and Y. Wang, *Phys. Rev. B* 54, 16533 (1996).
38. P. Giannozzi, S. Baroni, N. Bonini, M. Calandra, R. Car, C. Cavazzoni, D. Ceresoli, G.L. Chiarotti, M. Cococcioni, I. Dabo, A.D. Corso, S. de Gironcoli, S. Fabris, G. Fratesi, R. Gebauer, U. Gerstmann, C. Gougoussis, A. Kokalj, M. Lazzeri, L. Martin-Samos, N. Marzari, F. Mauri, R. Mazzarello, S. Paolini, A. Pasquarello, L. Paulatto, C. Sbraccia, S. Scandolo, G. Sclauzero, A.P. Seitsonen, A. Smogunov, P. Umari, and R.M. Wentzcovitch, *J. Phys. Conden. Matter* 21(39), 395502 (2009).
39. J. Bardeen and W. Shockley, *Phys. Rev.* 80, 72 (1950).
40. F. Beleznay, F. Bogár, and J. Ladik, *J. Chem. Phys.* 119(11), 5690 (2003).
41. C. Ataca, H. Sahin, E. Akturk, and S. Ciraci, J. Phys. Chem. C 115(10), 3934 (2011).
42. P. Johari and V.B. Shenoy, *ACS Nano* 6(6), 5449 (2012).
43. J. Wilson and A. Yoffe, *Adv. Phys.* 18(73), 193 (1969).
44. H. RamakrishnaMatte, A. Gomathi, A. Manna, D. Late, R. Datta, S. Pati, and C. Rao, *Angew. Chem. Int. Ed.* 49(24), 4059 (2010).
45. A. Lu and R. Zhang, *Solid State Commun.* 145(5), 275 (2008).
46. C. Zhang, A. De Sarkar, and R.Q. Zhang, *J. Phys. Chem. C* 115(48), 23682 (2011).
47. J.W. Jiang, H.S. Park, and T. Rabczuk, *Nanoscale* 6(7), 3618 (2014).
48. Y. Cai, G. Zhang, and Y.W. Zhang, *J. Am. Chem. Soc.* 136(17), 6269 (2014).
49. W.S. Yun, S.W. Han, S.C. Hong, I.G. Kim, and R J.D. Lee, *Phys. Rev. B* 85, 033305 (2012).